Electronic Supplementary Material (ESI) for Journal of Materials Chemistry A.
This journal is © The Royal Society of Chemistry 2021

In-Situ Formation of Polymer Electrolytes Using a Dicationic Imidazolium Cross-linker for High-Performance Lithium Ion Batteries

Yu-Chao Tseng[a,b], *Shih-Hsien Hsiang*[a,b], *Chih-Hao Tsao*[a,c], *Hsisheng Teng*[a,b,*], *Sheng-Shu Hou*[a,b,*] *and Jeng-Shiung Jan*[a,b,*]

[a]Department of Chemical Engineering, National Cheng Kung University, Tainan 70101, Taiwan

[b]Hierarchical Green-Energy Materials (Hi-GEM) Research Center, National Cheng Kung University, Tainan 70101, Taiwan

[c]Rising Chemical Ltd. Co., Xiaogang Dist., Kaohsiung, 81264, Taiwan

*Correspondence: Hsisheng Teng, Department of Chemical Engineering, National Cheng Kung University, No. 1 University Road, Tainan City 701, Taiwan, E-mail: hteng@mail.ncku.edu.tw, Phone: 886-6-275-7575 ext 62640, Fax: 886-6-234-4496.; Sheng-Shu Hou, Department of Chemical Engineering, National Cheng Kung University, No. 1 University Road, Tainan City 701, Taiwan, E-mail: sshou@mail.ncku.edu.tw, Phone: 886-6-275-7575 ext 62641, Fax: 886-6-234-4496.; Jeng-Shiung Jan, Department of Chemical Engineering, National Cheng Kung University, No. 1 University Road, Tainan City 701, Taiwan, E-mail: jsjan@mail.ncku.edu.tw, Phone: 886-6-275-7575 ext 62660, Fax: 886-6-234-4496.

Experiments

Materials

1-vinyllimidazole, bromoethane and 1,4-diiodobutane were supplied from Alfa Aesar. Poly(ethylene glycol) methyl ether methacrylate (PEGMEA) (Mn = 500 g/mol), poly(ethylene glycol) dimethyl ether (PEGDME) (Mn = 500 g/mol), sodium sulfate, polyvinylidene difluoride (PVDF) and 2,2′-azobis(2-methylpropionitrile) (AIBN) were obtained from Sigma Aldrich. Charcoal activated was received from Tokyo Chemical Industry company. Lithium bis(trifluoromethylsulfonyl) (LiTFSI) was provided by Solvay and kept in the glove box. Lithium metal and aluminum foil were purchased from UBIQ company. $LiFePO_4$ and super P were used as received from Timcal and Aleees, respectively. All the used solvents were ACS reagent grade.

Synthesis of prepolymers (VIm-TFSI and XVIm-TFSI)

VIm-TFSI was synthesized by refluxing a solution of 1-vinyllimidazole (1 mmol) and bromoethane (1.2 mmol) in ethyl acetate overnight. The bromide intermediate was collected from the mixture at the end of the reaction. After stirring with ethyl acetate (3 times) to remove any unreacted impurity, the intermediate was then dissolved in water followed by adding excessive LiTFSI into the solution. The mixtures were stirred for another 5 hours. After the reaction, the clarify liquid precipitated was poured in ethyl acetate and extracted with water until the residual LiBr would not be detected by 0.1M $AgNO_3$ aqueous solution. The combined organic layer was dried over sodium sulfate and purified by passing through charcoal activated. The solvent was then concentrated by rotary evaporation and dried under vacuum at 80 ^oC overnight to yield the desired prepolymer, VIm-TFSI. XVIm-TFSI was obtained via a similar procedure except the added

bromoethane was replaced by 1,4-diiodobutane, and the molar ratio between 1-vinyllimidazole and 1,4-diiodobutane was set as 1: 0.4. The synthesis procedure is illustrated in Figure S1.

Electrolyte Preparation

The electrolytes were prepared by in-situ polymerization. First, the mixtures with desired amount of VIm-TFSI or XVIm-TFSI/PEGMEA/LiTFSI/PEGDME were dissolved together in an argon filled glove box. The weight ratio of prepolymer, LiTFSI and PEGDME was set as 5: 3: 4, while the weight percentage of VIm-TFSI or XVIm-TFSI was between 10 - 25 % based on the total prepolymer mass. P-10, for instance, was prepared as follows. VIm-TFSI (20 mg), PEGMEA (180 mg), LiTFSI (120 mg), PEGDME (160 mg) and AIBN (6 mg) were mixed for 3 hours to form a homogeneous solution, which was dropped on the lithium metal directly. Then the in-situ polymerization was performed upon a hot plate at 70 ^{o}C for 6 hours in the glovebox, a transparent electrolyte sticking to the lithium anode was thus obtained. Other products were prepared through the method same as that of P-10 only the contents of VIm-TFSI or XVIm-TFSI were modified to the corresponding values, and a control sample (P-0) without cationic segments was also synthesized for comparison. All electrolyte compositions were recorded in Table S1.

Characterization

^{1}H nuclear magnetic resonance spectroscopy (^{1}H NMR) was performed on a Bruker Avance 600NMR with dimethyl sulfoxide-d^{6} as solvent. Fourier transform infrared spectroscopic (FT-IR) measurement was conducted on a Thermo Nicolet Nexus 6700. The surface morphology of materials was probed through Hitachi SU8010 Field-Emission Scanning Electron Microscopy (FE-SEM) with an accelerating voltage of 10 kV. The samples were mounted on a platform and sputtered with Pt for 3 mins before observations. X-ray diffraction (XRD) analysis was characterized by a Rigaku Ultima IV-9407F701 X-ray spectrometer with Cu

Kα (0.154 nm) radiation operating at 50 kV and 250 mA. Thermogravimetric analysis (TGA) was conducted on a Perkin-Elmer TGA 4000 under a nitrogen atmosphere from 25 ^{o}C to 600 ^{o}C at the rate of 15 ^{o}C min^{-1}. The calorimetric measurement was run on a differential scanning calorimeter (DSC) with a TA Instruments Q100. Samples were sealed in aluminum pans and heated/cooled at a rate of 10 °C min^{-1} under a nitrogen atmosphere. The elastic modulus of each sample was measured via the compression test using a dynamic mechanical analyzer (ARES G2) from 0 to 60 % strain at a rate of 0.01 mm s^{-1}. The samples were cylindrical, with a 2: 1 ratio of diameter: thickness (10.0 mm: 5.0 mm). And the value of the compression modulus was calculated from the slope of the stress-strain plot.

Ionic conductivity measurements were conducted via AC impedance spectroscopy, using a CH Instruments 6116E at open circuit voltage in the frequency range of 10^{-1} Hz to 10^{6} Hz at temperatures from 25 °C to 80 °C. A feeler gauge was used to measure the thickness (D) of the samples which were then sandwiched between two stainless steels for the measurement. An extrapolation was adopted based on the ten plots at the high frequency end and the x-axis value of the intersection was defined as the bulk resistance of the electrolyte (R). The ionic conductivity of electrolytes can thus be calculated through the following equation:

$$\sigma\left(\frac{S}{cm}\right) = \frac{D}{RA}$$

where R represents the obtained bulk resistance, D and A are the thickness (cm) of the electrolyte and the contact area (cm^2) of the stainless steel/electrolyte, respectively. The electrochemical stability window of the electrolytes was studied by a linear sweep voltammetry (LSV) technique in a cell that sandwiched the sample between lithium metal and a stainless steel disk, in which the lithium metal was employed as the reference and counter electrode while the stainless steel was employed as the working electrode,

respectively (scan rate: 5 mV s^{-1}). The interfacial compatibility between the electrolyte and lithium anode was evaluated through lithium plating/stripping cycling test using symmetrical lithium coin cells at the BAT-700 battery testing system. Charge-discharge cycling was performed at different current densities ranged from 50 μA cm^{-2} to 300 μA cm^{-2} to determine the limit value and it was kept at a constant current density of 100 μA cm^{-2}, for each polarization (3 hours charge and 3 hours discharge). Li/$LiFePO_4$ cells based on lithium metal anode, $LiFePO_4$ cathode (80 wt% active material ($LiFePO_4$), 10 wt% binder (PVDF) and 10 wt% conductive agent (Super P)) and the as-prepared electrolytes were assembled in an argon-filled glove box. The $LiFePO_4$ loading was 2.4 ~ 3.0 g cm^{-2} for each cathode. The charge-discharge performance, rate capacity and cycle life of the cells were assessed on the battery testing system (BAT-750B) from 2.5 V to 4.0 V at 25 ^oC and 60 ^oC, respectively, and a 30-second rest time was set between each cycle. At 1st, 25th, 50th, 75th, and 100th cycles, the cells were dismounted from the fixture and connected to CH Instruments 6116E for AC impedance measurements. Afterwards, they were mounted back on the fixture again for continuous charge-discharge cycling and the cells were disassembled after cycling to observe the surface morphology of lithium anode.

Table S1. The composition of the prepared electrolytes.

Electrolyte		Weight (mg)				
		Prepolymer			LiTFSI	PEGDEM
		VIm-TFSI	XVIm-TFSI	PEGMEA		
Control Sample, P-0		-	-	200	120	160
P-series	P-10	20	-	180	120	160
	P-15	30	-	170	120	160
	P-20	40	-	160	120	160
	P-25	50	-	150	120	160
XP-series	XP-10	-	20	180	120	160
	XP-15	-	30	170	120	160
	XP-20	-	40	160	120	160
	XP-25	-	50	150	120	160

* Initiator (AIBN): 3 wt% of the prepolymers.

Table S2. Ionic conductivities, discharge capacities, compressive elastic modulus, and 5 % weight loss temperatures of P-20 and XP-20.

Sample	Ionic Conductivity (log (S/cm))		Discharge Capacity at 25°C (mAh/g)		Compressive Elastic Moduli (Mpa)		5% Weight Loss Temperature (T_d 5%) (°C)
	25°C	60°C	0.1C	1C	5 % strain	15 % strain	
P-20	-3.53	-3.04	168.2	70.0	0.006	0.010	239
XP-20	-3.63	-3.10	164.0	98.6	0.032	0.052	279

Table S3. The corresponding simulated impedance parameters of Li/$LiFePO_4$ cells with P-20 and XP-20 in an equivalent circuit.

Sample	Cycle	R_b (Ω)	R_t (Ω)
P-20	1st	110	1320
	25th	100	1810
	50th	120	2390
	75th	120	1580
	100th	100	1860
XP-20	1st	150	730
	25th	130	1230
	50th	150	1480
	75th	120	1780
	100th	100	2040

Table S4. Summary of cycle performance of Li/$LiFePO_4$ cells with other reported polymer electrolytes.

Polymer Electrolyte Composition	Cycle Number	Discharge Capacity (Cathode Material: $LiFePO_4$)	Ref.
XP-20 PILs-co-PEG/PEGDME/LiTFSI	150 35 180 100	151 mAh g^{-1}/ 0.2 C (25°C) 118 mAh g^{-1}/ 0.5 C (25°C) 149 mAh g^{-1}/ 0.2 C (60°C) 150 mAh g^{-1}/ 0.5 C (60°C)	This work
Pyrrolidinium-based PILs/IL/LiTFSI	70	150 mAh g^{-1}/ 0.05 C (40°C)	1
Pyrrolidinium-based PILs/SN/LiTFSI	40 10, 10, 10	150 mAh g^{-1}/ 0.1 C (25°C) 150, 130, 120 mAh g^{-1}/ 0.1, 0.5, 1 C (25°C)	2
Pyrrolidinium-based PILs/PEG/LiTFSI	70	140 mAh g^{-1}/ 0.2 C (80°C)	3
Pyrrolidinium-based PILs/IL+EC/LiTFSI	-	130 mAh g^{-1}/ 1 C (22°C)	4
Guanidinium-based PILs/IL/LiTFSI	100	130 mAh g^{-1}/ 0.1 C (80°C)	5
Guanidinium-based PILs/IL/LiTFSI	70	115 mAh g^{-1}/ 0.1 C (80°C)	6
Tetraalkylammonium-based PILs/IL/LiTFSI	130	125 mAh g^{-1}/ 0.1 C (60°C)	7
Tetraalkylammonium-based PILs/IL/LiTFSI	50	135 mAh g^{-1}/ 0.1 C (60°C)	8
Tetraalkylammonium-based PILs/IL/LiTFSI	100	155 mAh g^{-1}/ 0.1 C (60°C)	9
Tetraalkylammonium-based PILs/IL/LiTFSI	100	140 mAh g^{-1}/ 0.1 C (60°C)	10
Pyridinium-based PILs/IL/LiTFSI	250	140 mAh g^{-1}/ 0.1 C (25°C)	11
Imidazolium-based PILs/IL/LiTFSI	50	160 mAh g^{-1}/ 0.1 C (40°C)	12
Imidazolium-based PILs/IL/LiTFSI	15	130 mAh g^{-1}/ 0.1 C (25°C)	13
Imidazolium-based PILs-co-PEG/PEG/LiTFSI	50	110 mAh g^{-1}/ 0.2 C (55°C)	14
TEGDMA/PEG/LiTFSI	100	138 mAh g^{-1}/ 0.1 C (25°C)	15
INSPM-60/LiTFSI	200	131 mAh g^{-1}/ 0.1 C (60°C)	16
LiPCSI/PEG	80	120 mAh g^{-1}/ 0.1 C (60°C)	17
LiSTFSI-co-PEG/Ethylene Carbonate	100 100	138 mAh g^{-1}/ 0.2 C (50°C) 126 mAh g^{-1}/ 0.5 C (50°C)	18
$(PPEGMEA\text{-}b\text{-}PS)_2$/$CH_3O$-PEG-PC/fumed SiO_2/LiTFSI	100 100	138 mAh g^{-1}/ 0.2 C (28°C) 111 mAh g^{-1}/ 0.5 C (28°C)	19
PEG-CCH/LiTFSI	100	138 mAh g^{-1}/ 0.1 C (60°C)	20

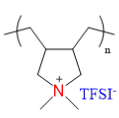

Pyrrolidinium-based PILs

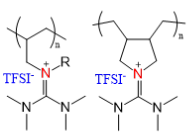

Guanidinium-based PILs

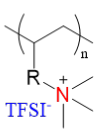

Tetraalkylammonium-based PILs

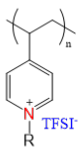

Pyridinium-based PILs

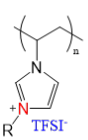

Imidazolium-based PILs

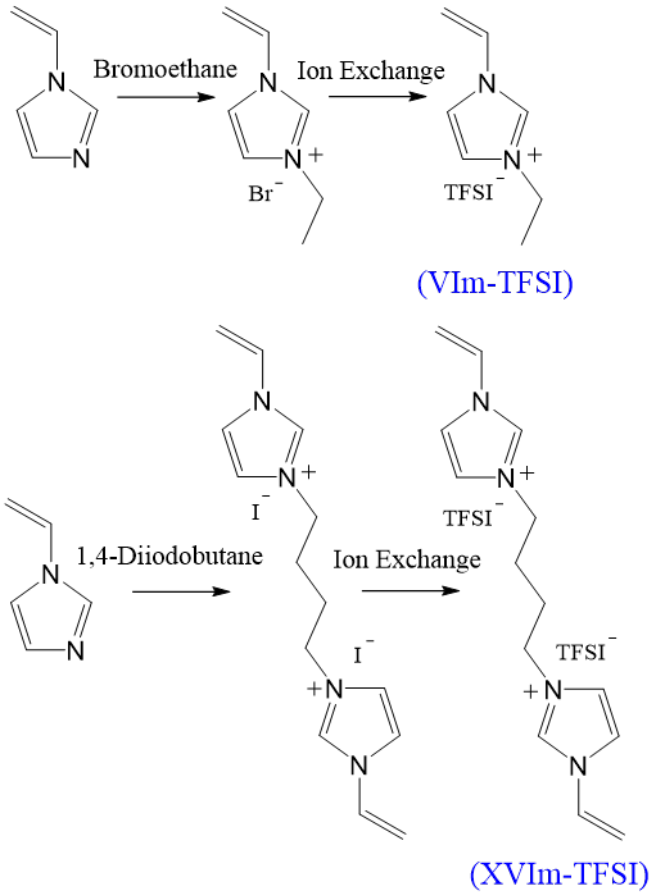

Figure S1. Synthesis of prepolymers, VIm-TFSI and XVIm-TFSI.

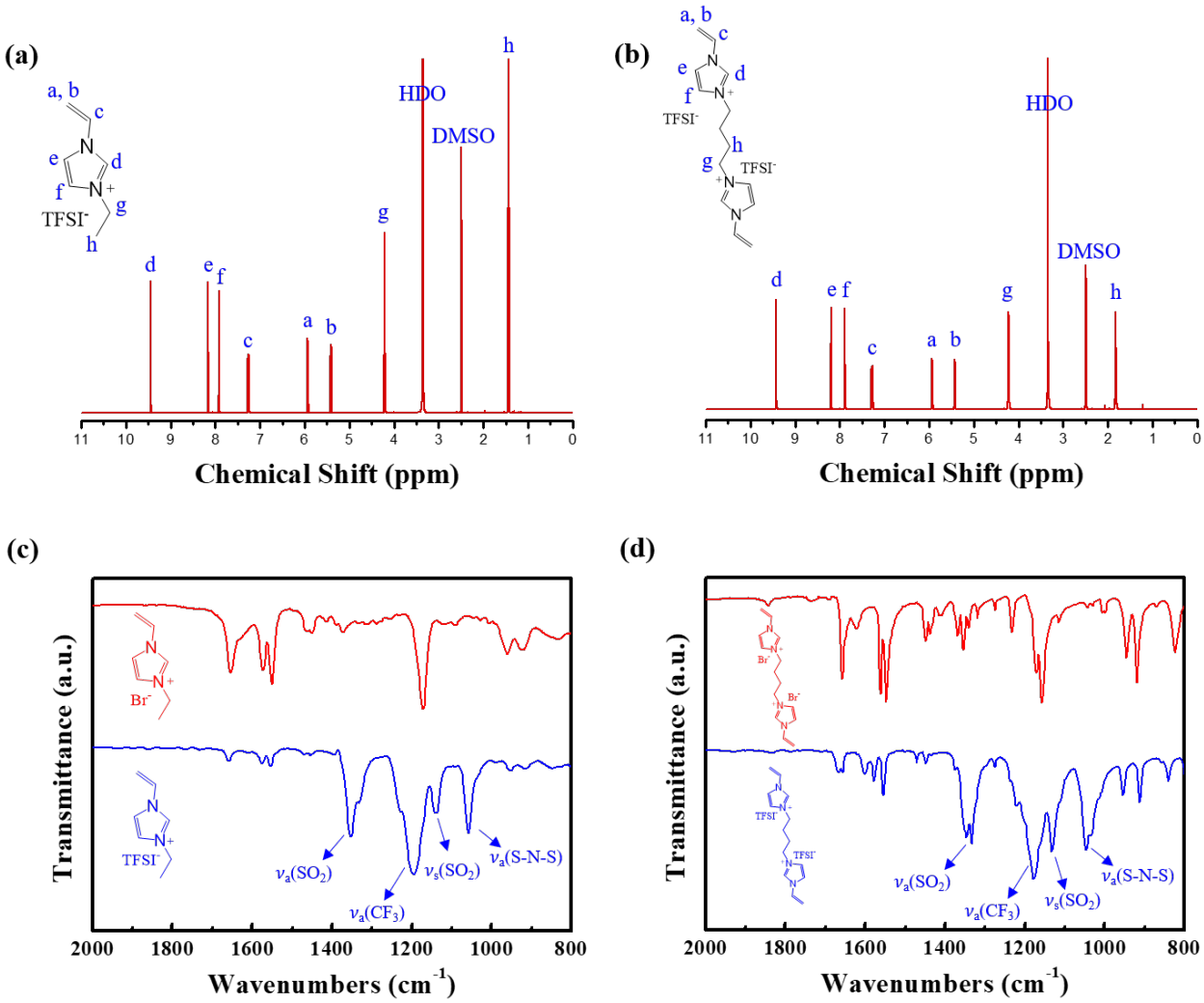

Figure S2. ^{1}H NMR spectra of the prepolymer (a) VIm-TFSI and (b) XVIm-TFSI. FT-IR spectra of the prepolymer (c) VIm-TFSI and (d) XVIm-TFSI before and after ion exchange.

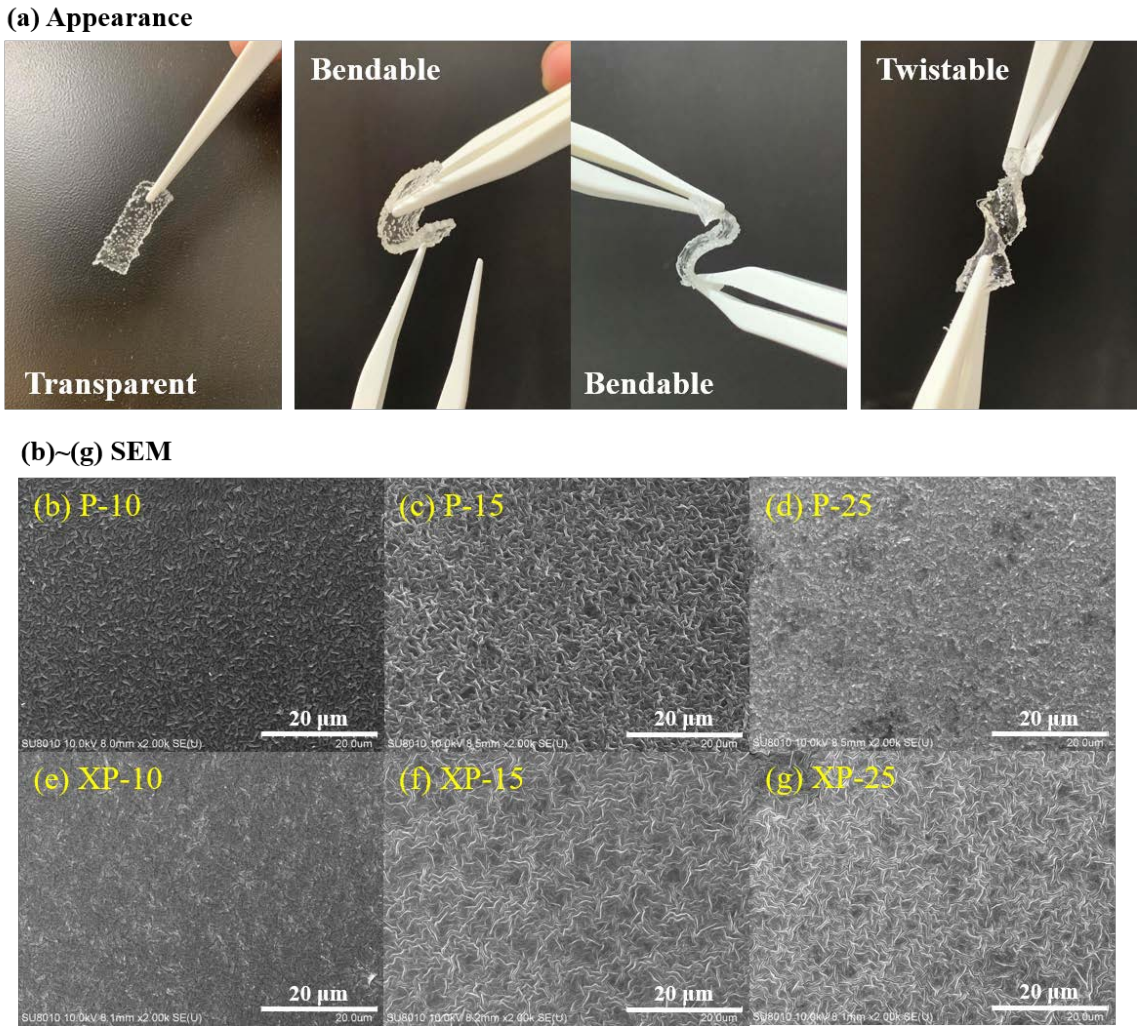

Figure S3. (a) Digital photographs of XP-20. (b)-(f) SEM photos of the electrolytes.

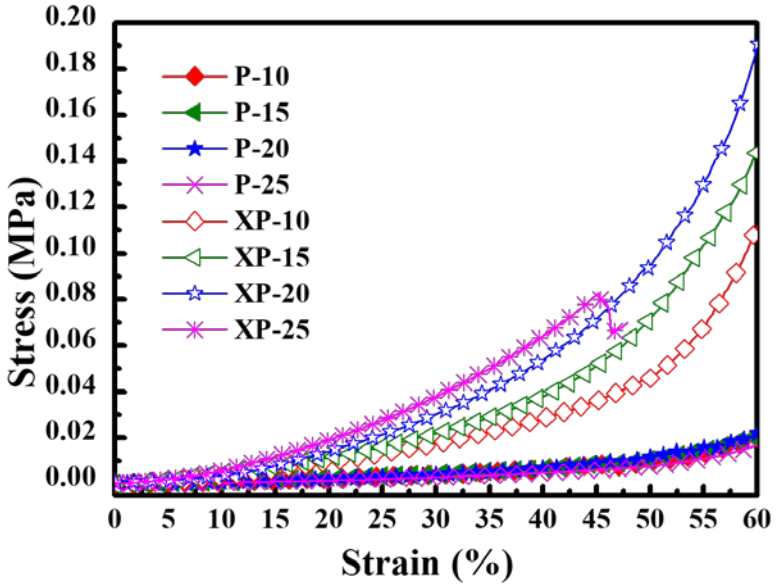

Sample	Compressive Elastic Moduli (Mpa)	
	5% strain	15% strain
P-10	0.006	0.010
P-15	0.006	0.010
P-20	0.006	0.010
P-25	0.003	0.007
XP-10	0.022	0.043
XP-15	0.032	0.052
XP-20	0.034	0.053
XP-25	0.041	0.079

Figure S4. Compressive stress-strain curves (cylindrical sample, 10.0 mm diameter × 5.0 mm thickness) and the calculated compressive elastic moduli of the electrolytes. Note that the XP-25 sample breaks at a strain of 45 %.

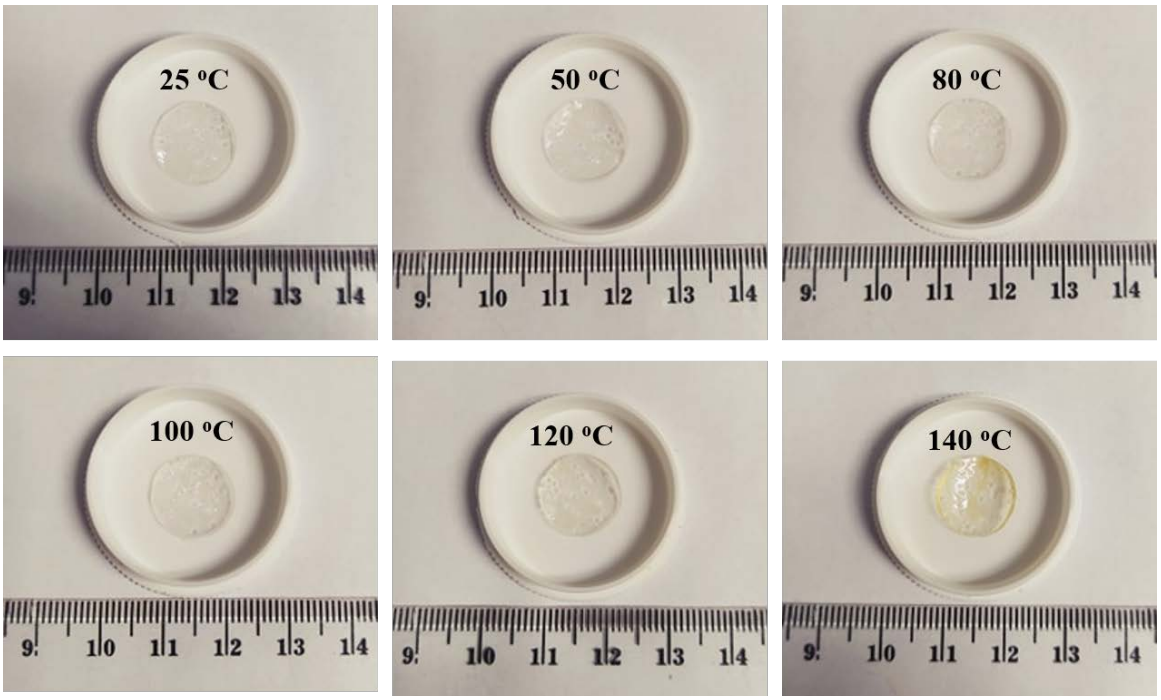

Figure S5. Photographs of a XP-20 sample after been heated to various temperatures (Each temperature was maintained for 2 hrs.).

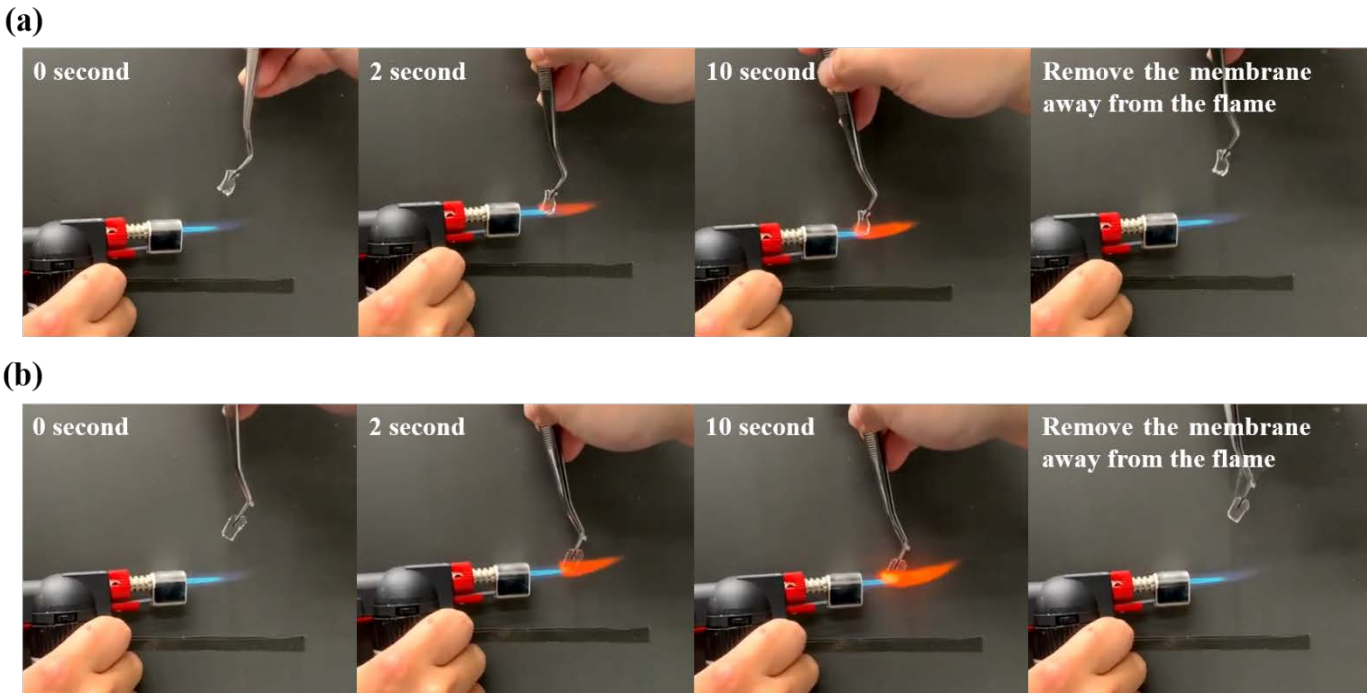

Figure S6. Combustion test for (a) P-20 and (b) XP-20 as a function of time. At 0 second, the flame started to ignite the membrane. After 2 seconds, both membranes started burning from the rim. After 10 seconds, remove the membrane away from the flame, and the membrane was self-extinguished immediately.

.

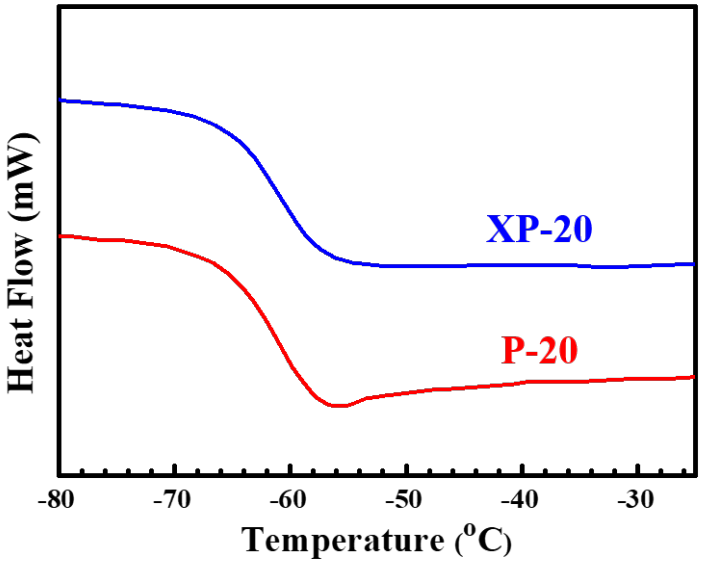

138

139 **Figure S7.** DSC curves of P-20 and XP-20. The inflection point was taken as T_g.

140

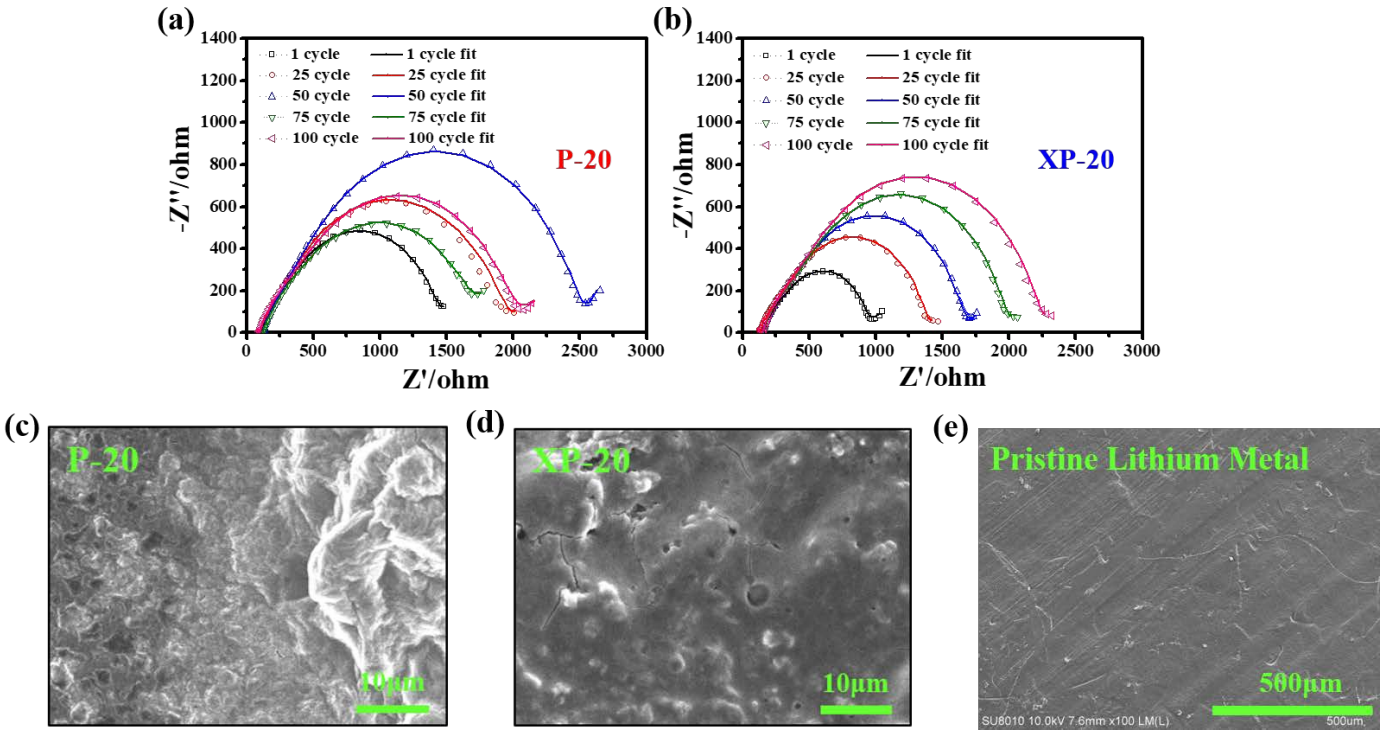

Figure S8. Electrochemical impedance spectra (EIS) of the Li/$LiFePO_4$ cells with (a) P-20 and (b) XP-20 after 1 cycle, 25 cycles, 50 cycles, 75 cycles and 100 cycles at 0.2 C rate at 25 ^oC. SEM photos of the lithium anode surface obtained from Li/$LiFePO_4$ cells with (c) P-20 and (d) XP-20 after cycling. (e) SEM images of the fresh lithium surface.

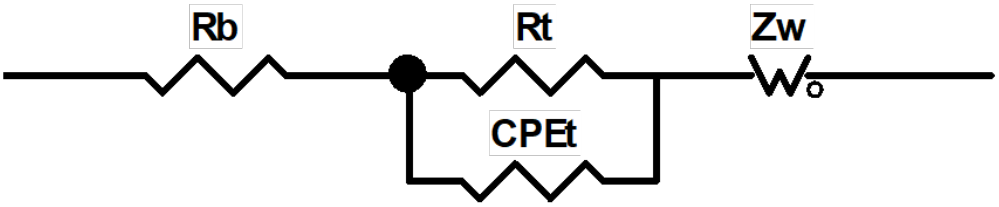

R_b: Bulk resistance of the cell.
R_t: Resistance of solid electrolyte interphase (SEI) (R_{sei}) and resistance of charge transfer at the interface between SEI and active materials (R_{ct}).
Z_w: Warburg impedance.

147

148 **Figure S9.** The equivalent circuit for the experimental EIS.

149

150

151

Reference

1. G. B. Appetecchi, G. T. Kim, M. Montanina, M. Carewska, R. Marcilla, D. Mecerreyes and I. De Meatza, *J Power Sources*, 2010, **195**, 3668-3675.
2. X. W. Li, Z. X. Zhang, S. J. Li, L. Yang and S. Hirano, *J Power Sources*, 2016, **307**, 678-683.
3. S. J. Li, Z. X. Zhang, K. H. Yang and L. Yang, *Chemelectrochem*, 2018, **5**, 328-334.
4. M. Safa, A. Chamaani, N. Chawla and B. El-Zahab, *Electrochim Acta*, 2016, **213**, 587-593.
5. M. T. Li, L. Yang, S. H. Fang, S. M. Dong, S. Hirano and K. Tachibana, *J Power Sources*, 2011, **196**, 8662-8668.
6. M. T. Li, L. Yang, S. H. Fang, S. M. Dong, S. Hirano and K. Tachibana, *Polym Int*, 2012, **61**, 259-264.
7. M. T. Li, B. L. Yang, L. Wang, Y. Zhang, Z. Zhang, S. H. Fang and Z. X. Zhang, *J Membrane Sci*, 2013, **447**, 222-227.
8. M. T. Li, L. Wang, B. L. Yang, T. T. Du and Y. Zhang, *Electrochim Acta*, 2014, **123**, 296-302.
9. Y. Zhou, B. Wang, Y. Yang, R. Li, Y. Wang, N. Zhou, J. Shen and Y. Zhou, *Reactive and Functional Polymers*, 2019, **145**, 104375.
10. N. Zhou, Y. Wang, Y. Zhou, J. Shen, Y. Zhou and Y. Yang, *Electrochim Acta*, 2019, **301**, 284-293.
11. X. L. Tian, Y. K. Yi, P. Yang, P. Liu, L. Qu, M. T. Li, Y. S. Hu and B. L. Yang, *Acs Appl Mater Inter*, 2019, **11**, 4001-4010.
12. K. Yin, Z. X. Zhang, X. W. Li, L. Yang, K. Tachibana and S. I. Hirano, *Journal of Materials Chemistry A*, 2015, **3**, 170-178.
13. P. F. Zhang, M. T. Li, B. L. Yang, Y. X. Fang, X. G. Jiang, G. M. Veith, X. G. Sun and S. Dai, *Adv Mater*, 2015, **27**, 8088-8094.
14. Y. H. Li, Z. J. Sun, L. Shi, S. Y. Lu, Z. H. Sun, Y. C. Shi, H. Wu, Y. F. Zhang and S. J. Ding, *Chem Eng J*, 2019, **375**, 121925.
15. Y. H. Zhang, W. Lu, L. N. Cong, J. Liu, L. Q. Sun, A. Mauger, C. M. Julien, H. M. Xie and J. Liu, *J Power Sources*, 2019, **420**, 63-72.
16. Y. F. Tong, H. L. Lyu, Y. Z. Xu, B. P. Thapaliya, P. P. Li, X. G. Sun and S. Dai, *Journal of Materials Chemistry A*, 2018, **6**, 14847-14855.
17. H. Y. Yuan, J. Y. Luan, Z. L. Yang, J. Zhang, Y. F. Wu, Z. G. Lu and H. T. Liu, *Acs Appl Mater Inter*, 2020, **12**, 7249-7256.
18. G. M. Luo, B. Yuan, T. Y. Guan, F. Y. Cheng, W. Q. Zhang and J. Chen, *Acs Applied Energy Materials*, 2019, **2**, 3028-3034.
19. T. Y. Guan, S. J. Qian, Y. K. Guo, F. Y. Cheng, W. Q. Zhang and J. Chen, *Acs Materials Letters*, 2019, **1**, 606-612.
20. Y. H. Jo, S. Q. Li, C. Zuo, Y. Zhang, H. H. Gan, S. B. Li, L. P. Yu, D. He, X. L. Xie and Z. G. Xue, *Macromolecules*, 2020, **53**, 1024-1032.